Inorg. Chem. **2002**, *41*, 2007–2013

Novel Chiral Three-Dimensional Iron(III) Compound Exhibiting Magnetic Ordering at $T_c = 40$ K

Donatella Armentano,[1a] Giovanni De Munno,*[,1a] Francesc Lloret,[1b] Andrei V. Palii,[†,1b] and Miguel Julve*[,1b]

Dipartimento di Chimica, Università degli Studi della Calabria, 87030 Arcavacata di Rende, Cosenza, Italy, and Departament de Química Inorgànica/Instituto de Ciencia Molecular, Facultat de Química de la Universitat de València, Avda. Dr. Moliner 50, 46100 Burjassot (València), Spain

Received October 22, 2001

The preparation and crystal structure determination of the iron(III) compound of formula $\{(NH_4)_2[Fe_2O(ox)_2Cl_2]\cdot 2H_2O\}_n$ (**1**) (ox = oxalate dianion) are reported here. Complex **1** crystallizes in the orthorhombic system, space group *Fdd*2, with $a = 14.956(7)$ Å, $b = 23.671(9)$ Å, $c = 9.026(4)$ Å, and $Z = 8$. The structure of complex **1** consists of the chiral anionic three-dimensional network $[Fe_2O(ox)_2Cl_2]^{2-}$ where the iron(III) ions are connected by single oxo and bisbidentate oxalato groups. The metal–metal separations through these bridging ligands are 3.384(2) and 5.496(2) Å, respectively. Ammonium cations and crystallization water molecules are located in the helical pseudohexagonal tunnels defined by iron atoms. The longest iron–iron distance in the pseudohexagonal tunnel is 15.778(2) Å whereas the shortest one is 8.734(2) Å. The iron atoms are hexacoordinated: a terminal chloro ligand and five oxygen atoms, that of the oxo group and four from two cis coordinated oxalate ligands, build a distorted octahedral environment around the metal atom. The Fe–O(oxo) bond distance [1.825(2) Å] is significantly shorter than the Fe(III)–O(ox) [average value 2.103(4) Å] and Fe(III)–Cl bond distances [2.314(2) Å]. Magnetic susceptibility measurements of **1** in the temperature range 2.0–300 K reveal the occurrence of a susceptibility maximum at 195 K and a transition toward a magnetically ordered state in the lower temperature region with $T_c = 40$ K. The strong antiferromagnetic coupling through the oxo bridge ($J = -46.4$ cm^{-1}, the Hamiltonian being $H = -JS_A\cdot S_B$) accounts for the susceptibility maximum whereas a weak spin canting of $\sim 0.3°$ due to the antisymmetric magnetic exchange within the chiral three-dimensional network is responsible for the magnetic ordering. The values of coercive field (H_c) and remnant magnetization (M_r) obtained from the hysteresis loop of **1** at 5 K are 4000 G and 0.016 μ_B.

Introduction

In the search for new molecular-based magnets during the past decade, the oxalate ion (hereafter noted ox) has appeared as a very appealing candidate because of its ability to mediate strong magnetic interactions between paramagnetic centers when adopting the bisbidentate coordination mode.[2] Recently, it has allowed the rational design of heterometallic two-dimensional (2D)[3−10] and three-dimensional (3D)[11−17] magnetic networks which exhibit ferro-, ferri-, or antiferromagnetic long-range ordering.[18−20] The hexagonal honeycomb topology is observed in the 2D compounds whereas helical networks are characteristic of the 3D ones. The synthetic strategy consists of polymerizing the tris-chelated $[M(ox)_3]^{(6-m)-}$ chiral mononuclear precursor into two or three directions, the formation of the 2D or 3D motif being dependent on the choice of the template counterion. The feasibility of an enantioselective synthesis of optically active 2D and 3D oxalate-bridged polymers using resolved $[Cr(ox)_3]^{3-}$ and $[M(bpy)_3]^{2+}$ (M = Ni, Ru; bpy = 2,2′-

* Authors to whom correspondence should be addressed. E-mail: miguel.julve@uv.es (M.J.); demunno@unical.it (G.De M.).
† On leave from the Quantum Chemistry Department, Institute of Chemistry, Academy of Sciences of Moldova, Academy Str. 3, MD-2028, Kishinev, Moldova.

(1) (a) Università degli Studi della Calabria. (b) Universitat de València.
(2) Kahn, O. *Molecular Magnetism*; VCH: Weinheim, Germany, 1993.
(3) Tamaki, H.; Zhong, Z. J.; Matsumoto, N.; Kida, S.; Koikawa, M.; Achiwa, N.; Hashimoto, Y.; Okawa, H. *J. Am. Chem. Soc.* **1992**, *114*, 6974.
(4) Atovmyan, L. O.; Shilov, G. V.; Lyubovskaya, R. N.; Zhilyaeva, E. I.; Ovanesyan, N. S.; Pirumova, S. I.; Gusakovskaya, I. G. *JETP Lett.* **1993**, *58*, 766.

10.1021/ic011100o CCC: $22.00
Published on Web 03/14/2002

bipyridine) species, which had been demonstrated only two years ago,[21] is an added value to these interesting magnetic materials.

Restricting ourselves to the oxalato−iron(III) system, only a few magneto-structural studies concerning either neutral[22] or anionic[23] dinuclear compounds are known. A relatively large antiferromagnetic coupling between the high spin iron(III) ions separated by more than 5.4 Å through bridging oxalato is observed (J up to -7.1 cm^{-1}). In the context of our current research work concerning the complex formation between trivalent first row transition metal ions and oxalate, we obtained the unprecedented chiral three-dimensional oxalato- and oxo-bridged iron(III) complex of formula $\{(NH_4)_2[Fe_2O(ox)_2Cl_2]\cdot 2H_2O\}_n$ (**1**) which exhibits a spin canted structure at low tempeature with $T_c = 40$ K.

We would like to finish this introduction with some comments on the connection between the spin canting and the antisymmetric exchange (AS) that is relevant to complex **1**. The exchange interactions for a pair of paramagnetic ions with spins S_A and S_B can be described in a general form by $H_{ex} = S_A J_{AB} S_B$; J_{AB} is a 3×3 tensor that contains the relevant exchange parameters. This tensor, J_{AB}, can be decomposed into a scalar J (describing the isotropic exchange and generally the dominating term), a traceless symmetric tensor, D_{AB}, (describing the anisotropic exchange), and an antisymmetric tensor.[24] The antisymmetric exchange term, which can be written as $G_{AB}[S_A \times S_B]$ where G_{AB} is an antisymmetric vector ($G_{AB} = -G_{BA}$), was introduced by Dzyaloshinsky[25] to explain the weak ferromagnetism of α-Fe_2O_3. The microscopic meanng of G_{AB} was elucidated by Moriya.[26] For systems without orbital degeneracy (as in high spin iron(III) ions), the AS exchange arises as a second-order contribution with respect to the spin−orbit coupling and isotropic exchange. Moriya formulated rules to specify the direction of G_{AB} for certain symmetries, and he proved that it vanishes when an inversion center is present in the pair A−B. Antisymmetric exchange has been frequently claimed for magnetically ordered states of extended lattices where it gives rise to the phenomenon of spin canting.[27] However, information about G_{AB} values for isolated complexes is very scarce.[28] The term $JS_A \cdot S_B$ leads to parallel or antiparallel alignment of S_A and S_B (depending on the nature of magnetic interaction, ferro or antiferromagnetic), whereas the $G_{AB}[S_A \times S_B]$ term tends to orient the spins pependicular to each other.[29] These competitive interactions between both terms yield a nonalignment of S_A and S_B (spin canting).

In this paper, we report the preparation, crystal structure, and magnetic study of the spin canted 3D system of formula $\{(NH_4)_2[Fe_2O(ox)_2Cl_2]\cdot 2H_2O\}_n$ (**1**).

Experimental Section

Materials. Iron(III) chloride and ammonium oxalate monohydrate were purchased from commercial sources and used as received. Elemental analyses (C, H, N) were performed by the Microanalytical Service of the Università degli Studi della Calabria.

Preparation of $\{(NH_4)_2[Fe_2O(ox)_2Cl_2]\cdot 2H_2O\}_n$ (1). Ammonium oxalate monohydrate (5 mmol) is added to an aqueous solution (50 mL) of iron(III) chloride (5 mmol). The mixture was gently warmed for 10 min, and the resulting deep yellow solution was allowed to stand at room temperature. Red plate crystals of **1** appeared after several days. The crystals were collected and washed with ethanol and diethyl ether. Yield about 30%. A second crop of green crystals of the compound $(NH_4)_3[Fe(ox)_3]\cdot 3H_2O$ were separated from the mother liquor. Anal. Calcd for $C_4H_{12}Cl_2Fe_2N_2O_{11}$ (**1**): C, 10.75; H, 2.71; N, 6.27. Found: C, 10.63; H, 2.64; N, 6.33. IR data [ν/cm^{-1}] on KBr pellets: 1670vs ν_{as}(O−C−O); 1349m and 1307s ν_s(O−C−O); 810m δ(O−C−O); 820m ν_{as}(Fe−O−Fe); 3588s,br and 3171s,br (H_2O).

Physical Techniques. The IR spectrum of **1** was obtained with a Perkin-Elmer 1750 FTIR spectrophotometer in the 4000−400 cm^{-1} region. Magnetic susceptibility and magnetization measurements were performed on a polycrystalline sample of **1** with a Quantum Design SQUID susceptometer covering the 2.0−300 K temperature range and using applied magnetic field ranging from 100 G to 5 T. The susceptometer was calibrated with $(NH_4)_2Mn(SO_4)_2\cdot 12H_2O$. The experimental susceptibility data of **1** were corrected for the diamagnetism estimated from Pascal's constants[30] [-176×10^{-6} cm^3 mol^{-1}].

(5) Decurtins, S.; Schmalle, H. W.; Oswald, H. R.; Linden, A.; Ensling, J.; Gütlich, P.; Hauser, A. *Inorg. Chim. Acta* **1994**, *216*, 65.
(6) Reiff, W. M.; Kreisz, J.; Meda, L.; Kirss, R. U. *Mol. Cryst. Liq. Cryst.* **1995**, *273*, 181.
(7) Mathonière, C.; Nuttall, C. J.; Carling, S. G.; Day, P. *Inorg. Chem.* **1996**, *35*, 1201.
(8) Carling, S. G.; Mathonière, C.; Day, P.; Abdul Malik, K. M.; Coles, S. J.; Hursthouse, M. B. *J. Chem. Soc., Dalton Trans.* **1996**, 1839.
(9) Pellaux, R.; Schmalle, H. W.; Huber, R.; Fischer, P.; Hauss, T.; Ouladdiaf, B.; Decurtins, S. *Inorg. Chem.* **1997**, *36*, 2301.
(10) Clemente-León, M.; Coronado, E.; Galán-Mascarós, J. R.; Gómez-García, C. J. *Chem. Commun.* **1997**, 1727.
(11) Decurtins, S.; Schmalle, H. W.; Schneuwly, P.; Oswald, H. R. *Inorg. Chem.* **1993**, *32*, 1888.
(12) Decurtins, S.; Schmalle, H. W.; Schneuwly, P.; Ensling, J.; Gütlich, P. *J. Am. Chem. Soc.* **1994**, *116*, 9521.
(13) Román, P.; Guzmán-Miralles, C.; Luque, A. *J. Chem. Soc., Dalton Trans.* **1996**, 3985.
(14) Decurtins, S.; Schmalle, H. W.; Pellaux, R.; Schneuwly, P.; Hauser, A. *Inorg. Chem.* **1996**, *35*, 1451.
(15) Decurtins, S.; Schmalle, H. W.; Pellaux, R.; Huber, R.; Fischer, P.; Ouladdiaf, B. *Adv. Mater.* **1996**, *8*, 647.
(16) Hernández-Molina, M.; Lloret, F.; Ruiz-Pérez, C.; Julve, M. *Inorg. Chem.* **1998**, *37*, 7, 4131.
(17) Coronado, E.; Galán-Mascarós, J. R.; Gómez-García, C. J.; Martínez-Agudo, J. M. *Inorg. Chem.* **2001**, *40*, 113.
(18) Okawa, H.; Matsumoto, N.; Tamaki, H.; Ohba, M. *Mol. Cryst. Liq. Cryst.* **1993**, *233*, 257.
(19) Decurtins, S.; Schmalle, H. W.; Pellaux, R.; Fischer, P.; Hauser, A. *Mol. Cryst. Liq. Cryst.* **1997**, *305*, 227.
(20) Day, P. In *Supramolecular Engineering of Synthetic Metallic Materials*; Veciana, J., Rovira, C., Amabilino, D. B., Eds.; NATO ASI Series C518; Kluwer: Dordrecht, The Netherlands, 1999; p 253.
(21) Andrés, R.; Gruselle, M.; Malézieux, B.; Verdaguer, M.; Vaissermann, J. *Inorg. Chem.* **1999**, *38*, 4637.
(22) (a) Julve, M.; Kahn, O. *Inorg. Chim. Acta*, **1983**, *76*, L39. (b) Lloret, F.; Julve, M.; Faus, J.; Journaux, Y.; Philoche-Levisalles, M.; Jeannin, Y. *Inorg. Chem.* **1989**, *28*, 3702.
(23) (a) Coronado, E.; Galán-Mascarós, J. R.; Gómez-García, C. J. *J. Chem. Soc., Dalton Trans.* **2000**, 205. (b) Rashid, S.; Turner, S.; Day, P.; Light, M. E.; Hursthouse, M. B. *Inorg. Chem.* **2000**, *39*, 2426. (c) Triki, S.; Bérézovsky, F.; Sala Pala, J.; Coronado, E.; Gómez-García, C. J.; Clemente, J. M.; Riou, A.; Molinié, P. *Inorg. Chem.* **2000**, *39*, 3771. (d) Armentano, D.; De Munno, G.; Faus, J.; Lloret, F.; Julve, M. *Inorg. Chem.* **2001**, *40*, 655.
(24) Bencini, A.; Gatteschi, D. *Electron Paramagnetic Resonance of Exchange Coupled Systems*; Springer-Verlag: Berlin, 1990.
(25) Dzyaloshinsky, I. *J. Phys. Chem. Solids* **1958**, *4*, 241.
(26) Moriya, T. *Phys. Rev.* **1960**, *120*, 91.
(27) Coffey, D.; Bedell, K. S.; Trugman, S. A. *Phys. Rev. B* **1990**, *42*, 6509.
(28) Kauffmann, K. E.; Popescu, C. V.; Dong, Y.; Lipscomb, J. D.; Que, L., Jr.; Münck, E. *J. Am. Chem. Soc.* **1998**, *120*, 8739.
(29) Erdös, P. *J. Phys. Chem. Solids* **1966**, *27*, 1705.

Table 1. Crystal Data and Structure Refinement for $\{(NH_4)_2[Fe_2O(ox)_2Cl_2]\cdot 2H_2O\}_n$ (**1**)

formula	$C_4H_{12}Cl_2Fe_2N_2O_{11}$
M	446.76
space group	*Fdd*2 (No. 43)
temp, K	293(2)
a, Å	14.956(7)
b, Å	23.671(9)
c, Å	9.026(4)
V, Å^3	3195(2)
Z	8
D_c, g cm^{-3}	1.857
μ, cm^{-1}	22.00
R1 [$I > 2\sigma(I)$][a]	0.0532
wR2[b]	0.1474

[a] $R1 = \sum||F_o| - |F_c||/\sum|F_o|$. [b] $wR2 = \{\sum[w(F_o^2 - F_c^2)^2]/[(w(F_o^2)^2]\}^{1/2}$.

Table 2. Selected Bond Lengths (Å) and Angles (deg)[a,b] for Compound **1**

Fe(1)−O(1)	1.825(2)	Fe(1)−O(2)	2.049(4)
Fe(1)−O(3)	2.194(4)	Fe(1)−O(4a)	2.052(4)
Fe(1)−O(5a)	2.116(4)	Fe(1)−Cl(1)	2.314(2)
O(1)−Fe(1)−O(2)	94.4(2)	O(1)−Fe(1)−O(4a)	102.1(2)
O(2)−Fe(1)−O(4a)	157.2(1)	O(1)−Fe(1)−O(5a)	92.0(1)
O(2)−Fe(1)−O(5a)	85.1(1)	O(4a)−Fe(1)−O(5a)	78.7(1)
O(1)−Fe(1)−O(3)	171.8(2)	O(2)−Fe(1)−O(3)	78.3(1)
O(4a)−Fe(1)−O(3)	84.0(1)	O(5a)−Fe(1)−O(3)	83.8(2)
O(1)−Fe(1)−Cl(1)	98.1(1)	O(2)−Fe(1)−Cl(1)	99.3(1)
O(4a)−Fe(1)−Cl(1)	93.9(1)	O(5a)−Fe(1)−Cl(1)	168.6(1)
O(3)−Fe(1)−Cl(1)	86.8(1)	Fe(1)−O(1)−Fe(1b)	135.9(4)

[a] Estimated standard deviations in the last significant digits are given in parentheses. [b] Symmetry transformations used to generate equivalent atoms: (a) $x - 1/4, -y + 1/4, z - 1/4$; (b) $-x, -y, z$.

X-ray Crystallographic Analysis. A crystal of **1** of dimensions 0.10 × 0.15 × 0.10 mm^3 was mounted on a Siemens R3m/V automatic four circle diffractometer and used for data collection. Diffraction data were collected at room temperature with graphite monochromated Mo Kα radiation ($\lambda = 0.71073$ Å) and using the $\omega-2\vartheta$ scan method. The unit cell parameters were determined from least-squares refinement of the setting angles of 25 reflections in the 2ϑ range 15°−30°. A summary of the crystallographic data and structure parameters are listed in Table 1. Examination of two standard reflections, monitored after every 50 reflections, showed no sign of crystal deterioration. Lorentz polarization corrections were applied to the intensity data.

The structure was solved by standard direct methods and subsequently completed by Fourier recycling. All non-hydrogen atoms were refined anisotropically except for the oxygen atom O(6) of the water molecule and the ammonium nitrogen atom N(1). Their hydrogen atoms were not located. The goodness-of-fit is 1.150. Solutions and refinements were performed with the SHELXTL NT system.[31] The final geometrical calculations were carried out with the PARST program.[32] The graphical manipulations were performed using the XP utility of the SHELXTL NT system. The main interatomic bond distances and angles are listed in Table 2.

Results and Discussion

Description of the Structure. The structure of **1** is made up of the anionic chiral three-dimensional network $[Fe_2O(ox)_2Cl_2]^{2-}$, ammonium cations, and crystallization water molecules. The iron atoms of this unprecedented network are bridged by a bischelating ox ligand and a single μ-oxo group, the chlorine atoms acting as terminal ligands. A fragment of this anionic motif with the atom-numbering scheme is shown in Figure 1. Electrostatic interactions, as well as hydrogen bonds involving the ammonium counterions, the oxalato groups, the coordinated chlorine atoms, and the crystallization water molecules, ensure the cohesion of the crystal lattice.

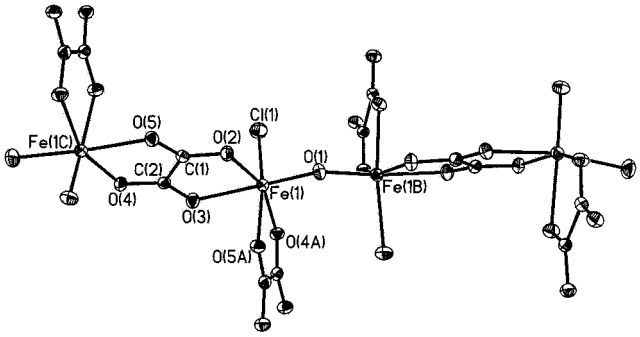

Figure 1. ORTEP drawing of a fragment of the anionic three-dimensional network of **1** showing the environment of the iron atom. Thermal ellipsoids are drawn at the 30% probability level.

Each iron atom is in a distorted octahedral environment, being bonded to four oxygen atoms of two cis oxalate groups, [O(2), O(3), O(4a), and O(5a) set of atoms], one oxygen atom of the μ-oxo group [O(1)], and one chlorine atom [Cl(1)]. The Fe−O(ox) [average value 2.103(4) Å] and Fe−O(μ-oxo) [1.825(2) Å] bond lengths are in agreement with those reported in the literature for other oxalato-[23,33] and oxo-bridged[34−37] iron(III) complexes. Also, the Fe−Cl bond length [2.314(2) Å] is in agreement with those reported for other similar compounds.[33,37,38]

The best equatorial plane around the iron atom is defined by the O(2), Cl(1), O(4a), and O(5a) set of atoms [largest deviation from the mean plane is 0.070 (2) Å at O(5a)], the iron atom being 0.248(3) Å out of this plane. The main distortion from the ideal octahedral geometry of the metal environment is due to the reduced bite angle of the ox ligand [78.3(1)° for O(2)−Fe(1)−O(3) and 78.7(1)° for O(4a)−Fe(1)−O(5a)]. The ox group is planar, and the carbon−carbon and carbon−oxygen bonds within this ligand are as expected. The iron atom is displaced by 0.052(5) Å out of this plane. The dihedral angle between the cis-coordinated oxalate groups is 84.2(1)° whereas that between two oxalates through the oxo bridge is 23.4(2)°. The Fe−O−Fe linkage is not linear, exhibiting an angle of 135.9(4)°. This value is the shortest one reported so far for this type of bridge [previous values ranging from 139° to 180°].[34−37] The iron−iron separation through the single oxo bridge is 3.384(2) Å

(30) Earnshaw, A. *Introduction to Magnetochemistry*; Academic Press: London, 1968.
(31) *SHELX NT*, version 5.1; Bruker Analytical X-ray Instruments Inc.: Madison, WI, 1998.
(32) Nardelli, M. *Comput. Chem.* **1983**, *7*, 95.
(33) Feist, M.; Troyanov, S.; Kemnitz, E. *Inorg. Chem.* **1996**, *35*, 3067.
(34) Murray, K. S. *Coord. Chem. Rev.* **1974**, *12*, 1.
(35) Kurtz, D. M., Jr. *Chem. Rev.* **1990**, *90*, 585.
(36) Matsushima, H.; Iwasawa, K.; Ide, K.; Reza, M. Y.; Koikawa, M.; Tokii, T. *Inorg. Chim. Acta* **1998**, *274*, 224 and references therein.
(37) Xiang, D. F.; Tan, X. S.; Zhang, S. W.; Han, Y.; Yu, K. B.; Tang, W. X. *Polyhedron* **1998**, *17*, 2095 and references therein.
(38) De Munno, G.; Ventura, W.; Viau, G.; Lloret, F.; Faus, J.; Julve, M. *Inorg. Chem.* **1998**, *37*, 1458.

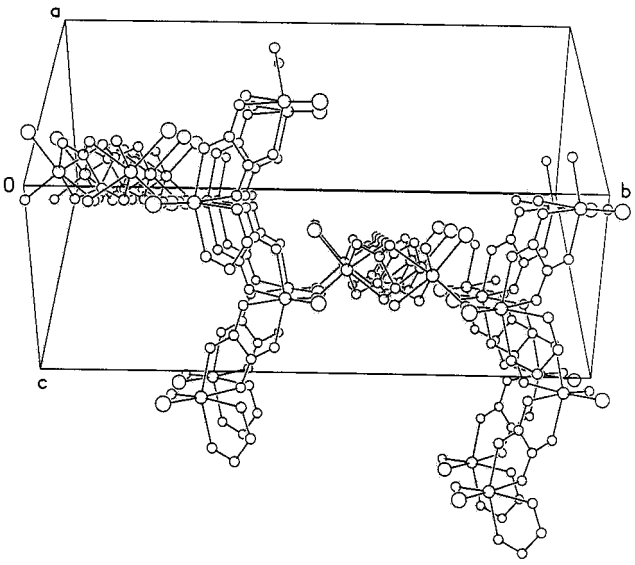

Figure 2. View of the crystal cell of **1** showing relative arrangement of the oxalato-bridged iron(III) chains connected through single oxo bridges.

[Fe(1)···Fe(1b)] whereas that through bridging oxalato is 5.496(2) Å [Fe(1)···Fe(1c); (c) = $x + {}^1/_4$, $-y + {}^1/_4$, $z + {}^1/_4$].

The chiral three-dimensional network is formed by oxalato-bridged iron(III) chains growing in the direction of the diagonal line of the *a* and *c* axes (see Figure 2) which are linked through a single oxo bridge to parallel planes containing only oxalato-bridged iron(III) chains. The dihedral angle between the planes and the chains is ∼62°. These motifs define helical tunnels, as shown in Figure 3. Two subunits, each one constituted of three iron atoms and two ox groups, linked to two others which contain only two iron atoms and one ox group by means of four μ-oxo bridges, build a pseudohexagonal motif. The longest Fe···Fe distance in the pseudohexagonal tunnel is 15.778(2) Å whereas the shortest one is 8.734(2) Å. The ammonium cations and crystallization water molecules are placed in these tunnels and are held together by means of hydrogen bonds [O(6)···N(1a) = 3.079(1) Å]. They are attached to the walls through hydrogen bonds involving the ammonium groups with some of the oxalato oxygens [O(3)···N(1d) = 3.024(1) Å, and O(5)···N(1c) = 3.048(1) Å; (d) = $x + {}^1/_4$, $-y + {}^1/_4$, $z - {}^3/_4$] and coordinated chlorine atoms [Cl(1)···N(1a) = 3.339(1) Å].

Magnetic Properties. The thermal dependence of the $\chi_M T$ product (χ_M being the magnetic susceptibility per one iron(III) atom) for compound **1** is shown in Figure 4. At room temperature, $\chi_M T$ is equal to 1.82 cm^3 mol^{-1} K, a value which is much smaller than that expected for a magnetically isolated spin sextet [4.38 cm^3 mol^{-1} K for $S_{Fe(III)} = {}^5/_2$ with $g = 2$]. Upon cooling, $\chi_M T$ decreases, and it attains a minimum at 40 K. Below this temperature, $\chi_M T$ increases abruptly to reach a maximum at 25 K, and in the very low-temperature range, $\chi_M T$ varies linearly with T, and it vanishes. The χ_M versus T plot for **1** exhibits a maximum at 195 K and a rapid increase for $T < 55$ K (see inset of Figure 4).

This abrupt increase both in χ_M and $\chi_M T$ in the low-temperature region can be attributed to a spin canting. In fact, the FCM (field-cooled magnetization) of **1** under 100 G, which is shown in Figure 5, reveals the occurrence of a magnetic ordering below 40 K, and the magnetization curve rapidly saturates at 0.023 μ_B. The magnetic hysteresis loop (see inset of Figure 5) shows values of the coercive field (H_c) and remnant magnetization (M_r) of 4000 G and 0.016 μ_B, respectively. From the saturation value of the magnetization (0.023 μ_B) and that expected for spin $S = {}^5/_2$ (5 μ_B), a value of the canting angle of ∼0.3° is easily derived. The spin canted structure is compatible with the structure of **1** because of the lack of inversion center. It is well-known that two mechanisms lead to spin canting: (i) magnetic anisotropy and (ii) antisymmetric exchange. Because of the isotropic character of the high spin iron(III) ion, the second factor has to be responsible for the canting in **1**, and it can proceed through the oxo and oxalato bridges because of the lack of inversion center in the Fe−O−Fe and Fe−ox−Fe pairs.

The oxo and oxalate groups are able to transmit strong antiferromagnetic interactions between the paramagnetic centers when acting as bridging ligands. In the case of the oxalato-bridged iron(III) complexes, the value of the exchange coupling J is basically constant (ca. -7 cm^{-1} with $H = -JS_A \cdot S_B$)[22,23] because of the rigidity of this type of bridge. The χ_M versus T plot of this type of complex shows a maximum around 27 K. As far as the more flexible single oxo-bridged iron(III) dinuclear complexes are concerned, the values of J are strongly dependent on the angle at the oxo bridge, and they are always much greater than those through the oxalato.[34−37] In this sense, the susceptibility maximum at 195 K which is observed in the χ_M versus T plot in **1** indicates that the antiferromagnetic interaction through the oxo bridge is dominant. Consequently, in a first approach, we analyze the high-temperature magnetic susceptibility data of **1** through the HDVV Hamiltonian (eq 1)

$$H = -JS_A \cdot S_B \qquad (1)$$

where J is the isotropic exchange parameter and S_A and S_B are the operators associated with the local spins ($S_A = S_B = {}^5/_2$). The best-fit parameters obtained through this simple model are $J = -46.3$ cm^{-1} and $g = 2.0$. However, this model (dotted line in Figure 6) hardly reproduces the experimental data. A large mismatch is observed between the experimental and calculated magnetic data for $T \leq 150$ K, the temperature range where the magnetic influence of the oxalato bridge is not relevant. In a second approach, we introduce the antisymmetric exchange (see Appendix) as the second term in eq 2[25,26]

$$H = -JS_A \cdot S_B + G \cdot [S_A \times S_B] \qquad (2)$$

where only two of the three components of the vector G (G_x and G_y) have to be considered in our system. In fact, in the structure of **1**, there is a 2-fold rotation axis (z axis) perpendicular to the AB line (segment connecting the two spins in the Fe−oxo−Fe fragment, xy plane) through the oxo atom. For such a situation, the rules concerning the direction of vector G state that G is perpendicular to the 2-fold rotation axis, and thus, $G_z = 0$, and G lies in the xy plane.[39] Using the irreducible tensor operators' technique (see

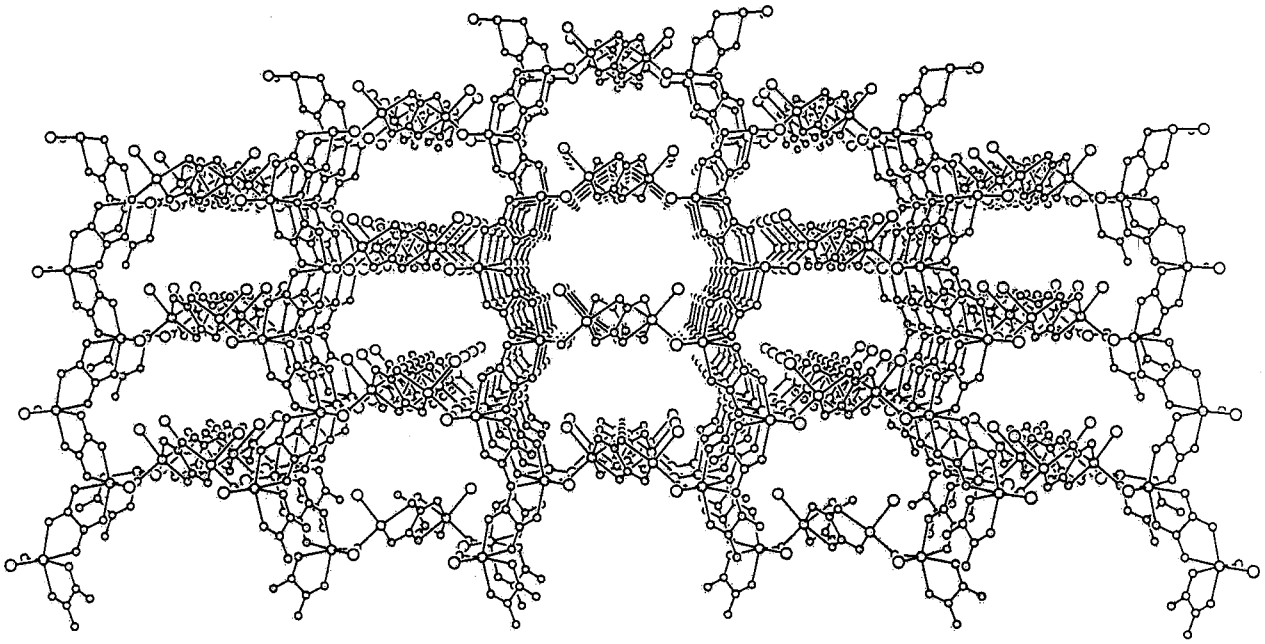

Figure 3. View of the chiral three-dimensional network of compound **1** in the direction of the diagonal line of the *a* and *c* axes. Ammonium cations and water molecules are omitted for the sake of clarity.

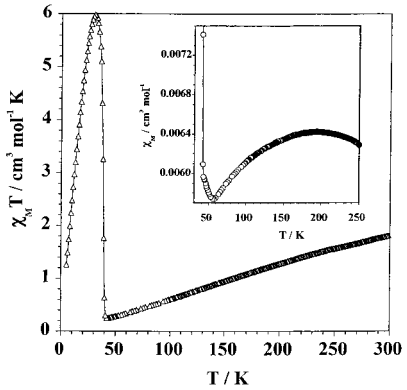

Figure 4. Thermal variation of the $\chi_M T$ product for compound **1** at 100 G. The inset shows the χ_M versus T plot for $T > 45$ K. The solid line is an eye guide.

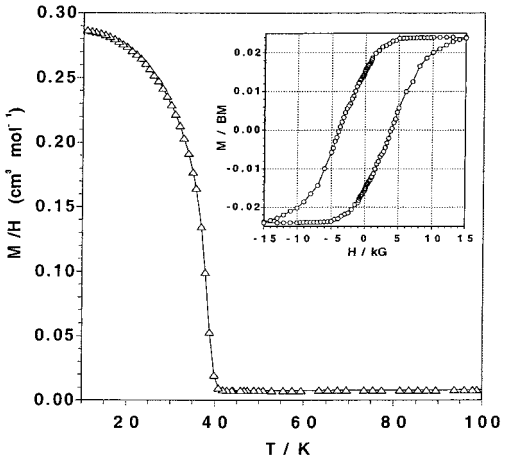

Figure 5. Plot of the field-cooled magnetization for compound **1** at $H =$ 100 G. The inset shows the hysteresis loop at 5 K.

Appendix) and making the reasonable assumption that $G_x = G_y$ (this precludes overparametrization in the best-fit procedure), we were able to reproduce well the susceptibility

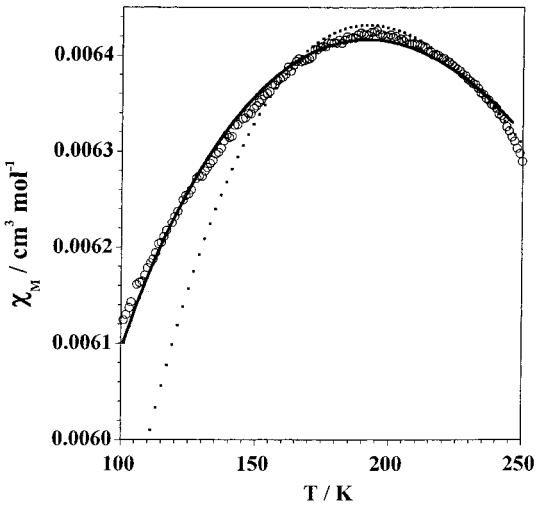

Figure 6. Thermal variation of χ_M of **1** in the high-temperature region: (○) experimental data; (···) and (–) best fits through eqs 1 and 2, respectively (see text).

data until 100 K (solid line in Figure 6), the best-fit parameters being $J = -46.4$ cm^{-1}, $G_x = G_y \equiv G = 3.6$ cm^{-1}, and $g = 2.0$. Below 100 K, the magnetic influence of the oxalato bridge is relevant, and this precludes the extension of our model to the data of this region. It deserves to be noted that the computed J and G parameters correspond only to the Fe−O−Fe pair and that it is also possible to have antisymmetric exchange through the oxalato bridge because of the lack of any symmetry element at the Fe−ox−Fe unit. Unfortunately, it is impossible to analyze this antisymmetric interaction because of the high dimensionality of **1**.

Information about values of G for isolated complexes is very scarce. Kauffmann et al.[28] obtained, from Mössbauer

(39) Yosida, K. *Theory of Magnetism*; Springer Series in Solid-State Sciences; Springer: Berlin, 1996; Vol. 122, p 58.

spectra, $G = 2.2$ cm^{-1} for a high spin iron(III) dinuclear complex with phenoxo and carboxylato groups as bridges. Rakitin et al.[40] deduced, from EPR spectra, $G = 1.4$ cm^{-1} for a high spin iron(III) trinuclear complex with oxo and carboxylato as bridges. Both values are of the same order of magnitude than that obtained for complex **1**.

A useful qualitative picture describing the physical consequences of the antisymmetric exchange in dinuclear complexes is the appearance of a canting angle (α) between the magnetic local moments (see Appendix). This angle can be calculated by eq 3 (eq A14 in Appendix):

$$\tan \alpha = (1/\sqrt{6})|G/J| \tag{3}$$

Thus, for isotropic antiferromagnetic exchange, a small antisymmetric exchange slants the adjacent spins and leads to weak magnetization in a direction perpendicular to the axis of the antiferromagnetic spin alignment (a noncollinear spin structure of the antiferromagnetically coupled spin pairs). The calculated value of α in the Fe−O(oxo)−Fe unit is 1.8°. The antiferromagnetic coupling through the oxalato bridge most likely contributes to reduce this canting angle at the three-dimensional level. This allows us to understand the smaller value of the canting angle for the bulk which is ~0.3° (value obtained from the saturation magnetization of **1**, 0.023 μ_B at 2 K).

Acknowledgment. Financial support from the Italian Ministero dell'Università e della Ricerca Scientifica e Tecnologica, the Human Capital and Mobility Program (Network on Magnetic Molecular Materials from EEC), through Grant ERBCHRX-CT920080 is gratefully acknowledged. One of us (A.V.P.) thanks the European Science Foundation, the Supreme Council of Science and Technological Development of Moldova (Grant N14), and the NATO Science Committee for financial support.

Appendix

Matrix Elements of the Antisymmetric Exchange and the Angle of Spin Canting. The antisymmetric exchange interaction between two magnetic centers A and B can be described by the effective spin-Hamiltonian:[24,41]

$$H_{AS} = G_{AB}[S_A \times S_B] = G_X[S_A \times S_B]_X + G_Y[S_A \times S_B]_Y + G_Z[S_A \times S_B]_Z \tag{A1}$$

where G_{AB} is an antisymmetric vector $G_{AB} = -G_{BA}$; G_X, G_Y, and G_Z are their cartesian components (in general different); and $[S_A \times S_B]$ is a vector product of S_A and S_B vectors. We will apply the relation between the spherical components $q = 0, \pm 1$ of the vector product and the irreducible tensor product of rank one:[24,41,42]

$$[S_A \times S_B]_q = -i\sqrt{2}\{S_1^A \otimes S_1^B\}_{1q} \tag{A2}$$

where $\{S_1^A \otimes S_1^B\}_1$ is the first rank irreducible tensor product of two spin irreducible tensor operators. Now, one can express the antisymmetric exchange Hamiltonian in terms of the irreducible tensor products:

$$H_{AS} = (G_Y - iG_X)\{S_1^A \otimes S_1^B\}_{1,-1} + (G_Y + iG_X)\{S_1^A \otimes S_1^B\}_{1,+1} - i\sqrt{2}G_Z\{S_1^A \otimes S_1^B\}_{1,0} \tag{A3}$$

The matrix element of the Hamiltonian A3, connecting the states characterized by the total spin S and its projection M (spin-coupled basis), can be calculated applying the formula given in ref 42 (p 479, eq 28). In this way, we obtain the following master formula:

$$\langle S_A S_B S'M'|H_{AS}|S_A S_B SM\rangle = [3(2S+1)S_A S_B(S_A+1)(S_B+1)(2S_A+1)(2S_B+1)]^{1/2} \times \begin{Bmatrix} 1 & 1 & 1 \\ S_A & S_B & S' \\ S_A & S_B & S \end{Bmatrix} [(G_Y - iG_X)\mathcal{O}^{S'M'}_{SM1-1} + (G_Y + iG_X)\mathcal{O}^{S'M'}_{SM11} - i\sqrt{2}\, G_Z\, \delta_{MM'}\mathcal{O}^{S'M}_{SM10}] \tag{A4}$$

where the conventional notations for the 9j-symbol and the Clebsch−Gordan coefficients are used.

Let us consider homonuclear dimers ($S_A = S_B \equiv S_0$) with antiferromagnetic ($J < 0$) isotropic exchange interaction described by the Hamiltonian:

$$H_{ex} = -JS_A S_B \tag{A5}$$

Equation A4 shows that the antisymmetric exchange mixes the ground spin-singlet state $|00\rangle$ with the excited spin-triplet states $|10\rangle$ and $|1\pm1\rangle$. Because G_X, G_Y, $G_Z \ll J$, the antisymmetric exchange can be treated as a perturbation, and the wave function of the ground state will take the form

$$|gr\rangle \approx |00\rangle + \frac{1}{J}\sum_{M=0,\pm1}\langle 1M|H_{AS}|00\rangle|1M\rangle \tag{A6}$$

Using the well-known properties of 9j- and 6j-symbols, we find

$$\begin{Bmatrix} 1 & 1 & 1 \\ S_0 & S_0 & 1 \\ S_0 & S_0 & 0 \end{Bmatrix} = \frac{(-1)^{2S_0}}{\sqrt{3(2S_0+1)}}\begin{Bmatrix} 1 & 1 & 1 \\ S_0 & S_0 & S_0 \end{Bmatrix} = \frac{1}{3(2S_0+1)\sqrt{2S_0(S_0+1)}} \tag{A7}$$

so

$$\langle 1M|H_{AS}|00\rangle = \frac{\sqrt{S_0(S_0+1)}}{\sqrt{6}}[(G_Y - iG_X)\delta_{M,-1} + (G_Y + iG_X)\delta_{M1} - i\sqrt{2}G_Z\delta_{M0}] \tag{A8}$$

Inserting eq A8 into eq A6, we arrive at the following final expression for the wave function of the ground state:

$$|gr\rangle = |00\rangle + \frac{\sqrt{S_0(S_0+1)}}{J\sqrt{6}}[(G_Y - iG_Z)|1-1\rangle + (G_Y + iG_Z)|11\rangle - i\sqrt{2}G_Z|10\rangle] \tag{A9}$$

(40) Rakitin, Y. V.; Yablokov, Y. V.; Zelentsov, V. V. *J. Magn. Res.* **1981**, *43*, 288.
(41) Tsukerblat, B. S.; Belinskii, M. I. *Magnetochemistry and Spectroscopy of Transition Metal Exchange Clusters*; Shtiintsa, Chisinau, Republic of Moldova, 1983.
(42) Varshalovich, D. A.; Moskalev, A. N.; Khersonskii, V. K. *Quantum Theory of Angular Momentum*; World Scientific: Singapore, 1988.

Because of the admixture of $S = 1$ states in the ground state, the mean value of the operators S_X^2 and S_Y^2 in the ground state prove to be nonzero. Defining

$$\langle S_\perp \rangle \equiv \sqrt{\langle gr|S_X^2 + S_Y^2|gr\rangle} = \sqrt{\langle gr|S^2 - S_Z^2|gr\rangle} \quad \text{(A10)}$$

one can find that

$$\langle S_\perp \rangle \equiv \frac{1}{|J|\sqrt{3}}\sqrt{S_0(S_0+1)(G_X^2 + G_Y^2 + 2G_Z^2)} \quad \text{(A11)}$$

In the classical limit, S_A and S_B can be regarded as the vectors that are antiparallel in the spin singlet ground state because of the antiferromagnetic isotropic exchange. On the other hand, $\langle S_\perp \rangle \neq 0$, so the antisymmetric exchange leads to the inclination (canting) of S_A with respect to S_B. This effect in the case of axial antisymmetric exchange ($G_X = G_Y = 0$) was analyzed by Erdös.[29]

In a classical spin model

$$\langle S_Z \rangle = \sqrt{S_0(S_0+1)} \quad \text{(A12)}$$

and we obtain the following result for the angle of spin canting:

$$\tan\alpha = \frac{\frac{1}{2}\langle S_\perp \rangle}{\langle S_Z \rangle} = \frac{1}{2|J|\sqrt{3}}\sqrt{G_X^2 + G_Y^2 + 2G_Z^2} \quad \text{(A13)}$$

One can see that the angle α is independent of the spin S_0. At the same time, the classical model for spins proves to be a good approximation, only providing large enough S_0 values as in the Fe(III)-dimer under consideration ($S_0 = {}^5/_2$). In the case of axial antisymmetric exchange, general formula A13 is simplified, and we arrive at the well-known result:[29,41]

$$\tan\alpha = \frac{1}{\sqrt{6}}|G/J| \quad \text{(A14)}$$

with $G_Z \equiv G$. Equation A14 is valid also providing $G_Z = 0$, $G_X = G_y \equiv G$ (the present case).

These results demonstrate that the antisymmetric exchange interaction leads to a perpendicular magnetization depending on the competition between the isotropic antiferromagnetic exchange resulting in the strictly antiparallel spin alignment and the antisymmetric exchange.

Supporting Information Available: X-ray crystallographic files in CIF format. This material is available free of charge via the Internet at http://pubs.acs.org.

IC011100O